Turkish Journal of Earth Sciences (Turkish J. Earth Sci.), Vol. 21, 2012, pp. 37–52. Copyright ©TÜBİTAK
doi:10.3906/yer-1007-33 First published online 20 April 2011

Al-in-Hornblende Thermobarometry and Sr-Nd-O-Pb Isotopic Compositions of the Early Miocene Alaçam Granite in NW Anatolia (Turkey)

ALTUĞ HASÖZBEK[1,2], BURHAN ERDOĞAN[3], MUHARREM SATIR[2], WOLFGANG SIEBEL[2], ERHAN AKAY[3], GÜLLÜ DENİZ DOĞAN[4,5] & HEINRICH TAUBALD[2]

[1] Dokuz Eylül University, Technical Vocational School of Higher Education, Natural Stone Technology, Torbalı, TR–35860 İzmir, Turkey (E-mail: altug.hasozbek@deu.edu.tr)
[2] Institut für Geowissenschaften, Universität Tübingen,Wilhelmstrasse 56, D-72074 Tübingen, Germany
[3] Dokuz Eylül University, Engineering Faculty, Department of Geological Engineering, Buca, TR–35160 İzmir, Turkey
[4] Hacettepe University, Department of Geological Engineering, Beytepe, TR–06800 Ankara, Turkey
[5] Université Blaise Pascal, OPGC, Lab. Magmas et Volcans, UMR-6524 CNRS, 5 rue Kessler, 63038, Clermont-Ferrand Cedex, France

Received 05 July 2011; revised typescripts received 31 January 2011 & 10 April 2011; accepted 20 April 2011

Abstract: During and after the closure of the Neo-Tethyan Ocean and progressive collision of the Tauride-Anatolide Platform with the Sakarya Continent, widespread magmatism occurred in NW Anatolia. This magmatism is manifested in a NW-trending belt along the northern border of the Menderes Massif. Due to the complex geodynamic setting of this region, the exact emplacement depth of the granitoids is still a matter of debate. Here we present Al-in-hornblende barometrical data and Sr-Nd-Pb isotope compositions of the Early Miocene Alaçam granite. The results imply a shallow emplacement depth of this granite (4.7±1.6 km) in contrast to previous studies which suggested emplacement along the brittle-ductile boundary of the crust. Furthermore, an evaluation of literature data let us reconsider the general emplacement mechanism of the Alaçam and other Early Miocene granitoids in the region. Initial isotopic signatures of the Alaçam granite are $^{87}Sr/^{86}Sr(I)$= 0.70865–0.70915, $e_{Nd}(I)$= –5.8 to –6.4, $\delta^{18}O$= 9.5–10.5, $^{206}Pb/^{204}Pb$ isotope ratios vary between 18.87 and 18.90. These features indicate an assimilation-dominated crustal crystallization and melt derivation from an older middle crustal protolith.

Key Words: Al-in-hornblende barometry, Sr-Nd-O-Pb isotopes, Alaçam granite, NW Anatolia

Erken Miyosen Yaşlı Alaçam Graniti'nin (KB Anadolu-Türkiye) Al-Hornblend Termobarometresi ve Sr-Nd-Pb-O İzotop Bileşimleri

Özet: Neo-Tetis okyanusunun kapanmasını izleyen Anatolid-Torid Platformu'nun Sakarya Kıtası ile progresif çarpışması sırasında ve sonrasında, KB Anadolu'da yaygın bir magmatizma meydana gelmiştir. Bu magmatizma, Batı Anadolu'da yer alan kuzey Menderes Masifi boyunca KB doğrultulu bir magmatik kuşak ortaya çıkarmaktadır. Bölgenin karmaşık jeodinamik evriminden dolayı, granitoidlerin yerleşim derinliği, halen tartışmalıdır. Bu çalışmada, Erken Miyosen yaşlı Alaçam granitinin Al-hornblend barometresi sonuçları ve Sr-Nd-Pb-O izotop bileşimleri sunulmaktadır. Elde edilen sonuçlar, Alaçam granitinin, önceki çalışmaların aksine, kabuğun sığ kesimlerinde (4.7±1.6 km) yerleştiğini ve önerilen kabuğun derin, elastik-plastik deformasyon sınırında gerçekleşen bir sokulum olmadığını belirtmektedir. Bununla beraber, literatürün yeniden değerlendirilmesiyle, Alaçam granitinin ve bölgedeki diğer Erken Miyosen granitoidlerinin yerleşim mekanizmasının yeniden incelenmesine neden olmuştur. Alaçam Graniti'nin birincil izotopik değerleri; $^{87}Sr/^{86}Sr(I)$= 0.70865–0.70915, $e_{Nd}(I)$= –5.8 to –6.4, $\delta^{18}O$= 9.5–10.5, $^{206}Pb/^{204}Pb$= 18.87–18.90'dır. Bu izotop verileri asimilasyonun baskın olduğu bir kabuksal kristallenmeyi ve granitin daha yaşlı bir orta kabuk köken kayasından türediğini göstermektedir.

Anahtar Sözcükler: Al-hornblend barometrisi, Sr-Nd-O-Pb izotopları, Alaçam graniti, KB Anadolu

Introduction

From Eocene to Quaternary time, extensive igneous activity took place in the Aegean-NW–W Anatolian region (Figure 1). Evolution of this widespread magmatic activity was studied by various researchers (Altherr & Siebel 2002; Altherr *et al.* 2004; Altunkaynak 2007; Brichau *et al.* 2007; Dilek & Altunkaynak 2007; Aydoğan *et al.* 2008; Özgenç & İlbeyli 2008; Akay 2009; İlbeyli & Kibici 2009; Erkül 2010; Hasözbek *et al.* 2010, 2011; Jolivet & Brun 2010; Stouraiti *et al.* 2010). In the Aegean Sea, S-type (i.e., Ikeria, eastern intrusion, Tinos-Krokos-Paros), and I-type granitoids (i.e., Tinos, Falatados, Ikeria, western intrusion, Naxos) are widely exposed, with extrusive and intrusive products. Miocene post-collisional I-type granitoids (i.e., Kozak, Evciler, Alaçam, Eğrigöz and Baklan) are also exposed in NW Anatolia along a belt straddling the southern and northern parts of the İzmir-Ankara Suture Zone (Figure 1). Petrogenetic models explaining this magmatic zone generally involve a mantle contribution during magma generation (Aldanmaz *et al.* 2000; Dilek & Altunkaynak 2007, 2009). Moreover, Aydoğan *et al.* (2008) found evidence for mantle and crustal-derived melt contribution in the genesis of the Baklan granite (Banaz-Uşak). Recent petrogenetic studies of the Miocene Eastern Aegean magmatism (Aegean island magmatism), however, are in basic agreement that those granitoids are derived from a crustal metasedimentary source (Altherr & Siebel 2002; Stouraiti *et al.* 2010). Stouraiti *et al.* (2010) suggested that three end members (metasedimentary biotite-gneiss, marble and amphibolite) were involved in the generation of the Middle–Late Miocene granitoids of the Aegean Sea. Various researchers have suggested petrogenetic models supporting this hypothesis, with new radiometric and structural data (Stouraiti *et al.* 2010 and references therein). The main purpose of these studies was to specify the geodynamic nature of this magmatism from Eocene to Quaternary time, namely to discover whether granite production was triggered by continent-continent collision, subduction of oceanic lithosphere, delamination, slab-break off, or by lithospheric extension along crustal detachments (Bozkurt & Oberhansli 2001; Altherr & Siebel 2002; Altherr *et al.* 2004; Altunkaynak 2007; Brichau *et al.* 2007; Dilek & Altunkaynak 2007, 2009; Aydoğan *et al.* 2008; Akay 2009; İlbeyli & Kibici 2009; Erkül 2010; Hasözbek *et al.* 2010, 2011; Jolivet & Brun 2010; Stouraiti *et al.* 2010).

This paper focuses on the Early Miocene Alaçam granitic body located along the northern border of the Menderes Massif (NW Anatolia) in the NW Anatolia Magmatic Belt. Geological, geochemical and geochronological results were published in Hasözbek *et al.* (2011). Here, we present new Al-in-hornblende thermobarometry and new Sr-Nd-O-Pb isotope data and present a model for the emplacement and the petrogenesis of the Alaçam granite. The petrogenesis and emplacement depth of the Alaçam granite are discussed in the frame of Early Miocene magmatism along the southern part of the İzmir-Ankara Suture Zone.

Regional Geological Setting

Tertiary magmatism in the eastern Mediterranean region, including both the Aegean Sea and NW Anatolia, was a consequence of different geodynamic processes (Dilek & Altunkaynak 2007, 2009; Jolivet & Brun 2010; Stouraiti *et al.* 2010). Major tectonic events occurring between Eocene and Quaternary time include subduction of the African lithospheric plate beneath the Aegean, collision between Africa and Eurasia, and backarc extension (e.g., Jolivet & Brun 2010; Stouraiti *et al.* 2010) (Figure 1). Both NW Anatolia and the Aegean islands have similar geological settings: in both regions blueschist facies metamorphism was almost entirely overprinted under high to medium temperature/low pressure metamorphic conditions (Okay 1980, 1982; Candan *et al.* 2005; Stouraiti *et al.* 2010). The metamorphic basement was intruded by the Eocene and Miocene granitoids (Karacık & Yılmaz 1998; Altunkaynak & Yılmaz 1999; Altunkaynak 2007; Dilek & Altunkaynak 2007, 2009; Akay 2009; Hasözbek *et al.* 2010, 2011) which are suggested to have been emplaced either along detachment faults in an extension zone (Bozkurt & Oberhänsli 2001; Işık & Tekeli 2001; Işık *et al.* 2003; Seyitoğlu *et al.* 2004; Ring & Collins 2005; Thomson & Ring 2006; Erkül 2010; Jolivet & Brun 2010; Stouraiti *et al.* 2010), or to have originated from a thickened crust resulting from a compression event (Karacık & Yılmaz 1998; Altunkaynak & Yılmaz 1999; Yılmaz *et al.* 2001; Yılmaz 2008; Akay 2009; Hasözbek *et al.* 2010, 2011).

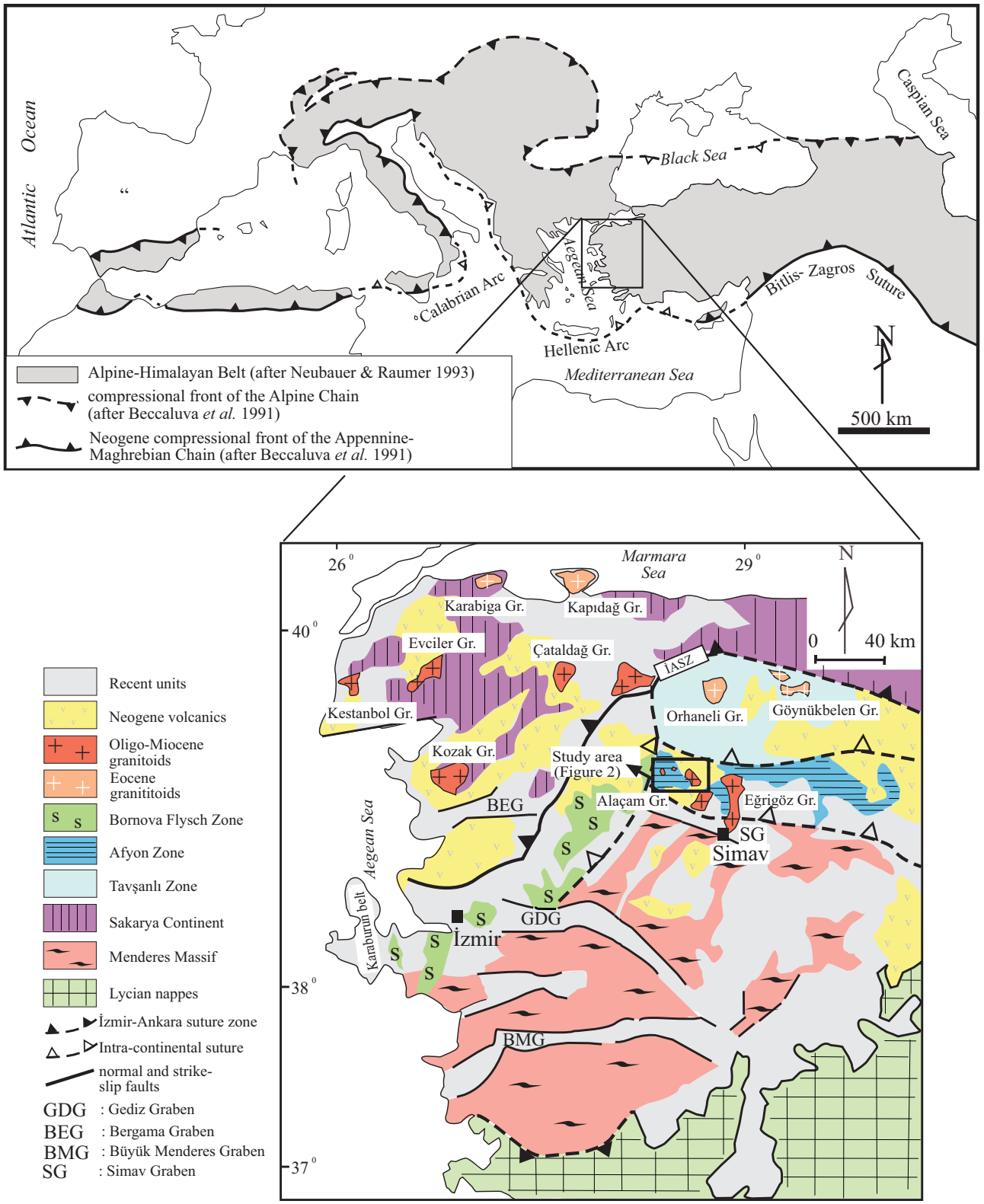

Figure 1. Generalized location of the Alpine-Himalayan Belt and location map of the study area (modified after Akal 2003; Hasözbek *et al.* 2010).

In NW Turkey, the Miocene Alaçam granite is exposed along the collision zone between the Sakarya Continent and the Menderes platform. The granite intrudes four different tectonic zones of these two continents which form imbricated nappe packages (Hasözbek *et al.* 2011) (Figures 1 & 2). These are, from bottom to top: (1) the Menderes metamorphics, characterized by a high- to medium-grade metapelite association, (2) a meta-ophiolitic nappe complex, similar in lithology to the Late Cretaceous Selçuk Formation (Güngör & Erdoğan 2001, 2002) which tectonically overlies the Menderes metamorphics, (3) the Afyon Zone, which tectonically overlies both the Menderes Massif and a meta-ophiolitic nappe complex (greenschist facies low-grade metamorphic rocks) comprising gneissic granites, metapelites, metarhyolites, and recrystallized limestones, and (4) the Bornova Flysch Zone, a non-metamorphic Late Cretaceous–Late Oligocene ophiolitic mélange, which tectonically overlies the Afyon Zone. The Alaçam granite and the tectonic package are unconformably overlain by Middle–Upper Miocene continental-lacustrine sedimentary rocks, and an andesitic volcanic sequence (Figure 2).

The granite and its related stocks yielded U-Pb zircon ages of 20.0±1.4 Ma and 20.3±3.3 Ma, respectively (Hasözbek *et al.* 2011) (Figure 2). The granite displays characteristically steeply-dipping, sharp contacts with the country rocks. The inner contact zone consists of microgranite, which gradually passes inward into a coarse-grained holocrystalline phase. Abundant enclaves of Menderes metamorphics and Afyon Zone rocks are found along the contact zone. The granitic body is not deformed, except in part of the contact zones, where it was probably caused by rapid cooling at a shallow crustal level during continuous emplacement (Hasözbek *et al.* 2011).

Analytical Methods

Geochemical analyses were carried out in Acme Analytical Laboratories Ltd (Vancouver, Canada) by ICP-AES (Inductively Coupled Plasma Atomic Emission Spectrometry) and ICP-MS (Inductively Coupled Plasma Mass Spectrometry). The data are published and discussed in detail in Hasözbek *et al.* (2011). Thin section preparation and polishing for microprobe analysis were done in the petrographical laboratory of Tübingen University, Germany. Chemical analysis of amphibole minerals from the Alaçam granite were carried out on a JEOL 8900 electron microprobe at the Institut of Geosciences, Tübingen University (Table 2). Raw data were corrected according to Armstrong (1991). Both synthetic and natural standards were used for calibration. The emission current was 15 nA and the acceleration voltage 15 kV. Counting times were usually 10 s for each element. In order to avoid significant Al increase through contact with plagioclase and biotite, analyses were performed on amphibole minerals in contact with quartz. The Anderson & Smith (1995) calibration method with temperature estimates from the plagioclase-hornblende geothermometer (reaction B) of Holland & Blundy (1994) was used where plagioclase was in contact with amphibole. Atomic proportions of amphiboles were taken from Holland & Blundy (1994). Pressure calculations, were performed by using excel sheet from Anderson & Smith (1995). Plagioclase compositions were determined by standard petrographical method. In plagioclase composition, dependence error was not more than ±0.5 kbar. Mineral BSE images were taken using the electron microprobe at the Institute of Geosciences, Tübingen University.

Sr, Nd, Pb, O isotope analysis from 6 samples of the Alaçam granite (Table 2) was performed at the Department of Geochemistry, Tübingen University. For Sr and Nd analyses, about 75–80 mg of whole-rock sample powder was spiked with mixed ^{84}Sr-^{87}Rb tracer. Samples were dissolved in concentrated HF acid in Teflon vials in poly-tetrafluor-ethylene (PTFE) reaction bombs at 220°C under high pressure for 4 days. Digested samples were dried and redissolved in 2.5 N HCL. Conventional cation exchange chromatography technique was used for separating Rb, Sr, Sm, Nd, U, Th and Pb. Sr was loaded with a Ta-HF activator and measured on a single W filament. Rb, Sm and Nd isotope compositions were measured in a double Re filament configuration mode and single Re filaments were used for Pb isotope measurements. Isotopic analyses were done using a Finnigan MAT 262 thermal ionization mass spectrometer (TIMS). For mass fractionation, Sr was normalized to $^{86}Sr/^{88}Sr$= 0.1194 and Nd was normalized to

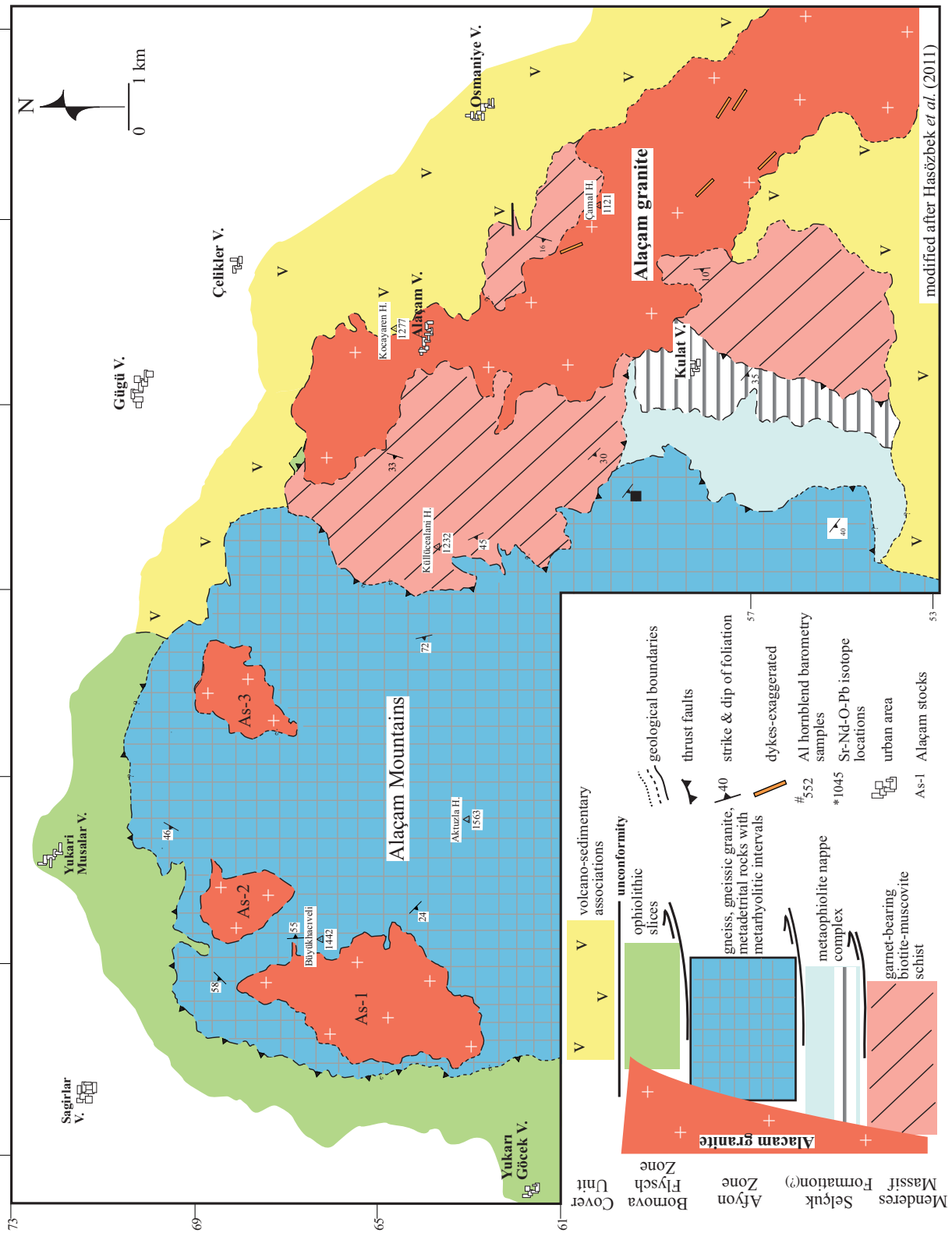

Figure 2. Geological map and columnar section of the study area (modified after Hasözbek *et al.* 2011).

$^{146}Nd/^{144}Nd$= 0.7219. During this study, measurement of the La Jolla Nd standard gave a mean $^{143}Nd/^{144}Nd$ ratio of 0.511820±10 (certified value of 0.511850) and NBS-987 Sr standard yielded a $^{87}Sr/^{86}Sr$ ratio of 0.710240±11 (certified value of 0.710245). $^{87}Rb/^{86}Sr$ ratios for whole rock samples were calculated from the $^{87}Sr/^{86}Sr$ ratios and the Rb and Sr concentrations taken from the ICP/ES measurements. The thermal fractionation of Pb isotopes was determined by measuring of Pb standard NBS981 and the isotopic ratios were corrected for 0.11% fractionation per atomic mass unit. All the initial isotopic calculations were based on the 20.0±1.4 Ma U-Pb zircon ages of the Alaçam granite (sample no: 1045) (Hasözbek *et al.* 2011).

Oxygen from whole-rock samples was extracted with BrF_5 according to the method of Clayton & Mayeda (1963). About 7 mg of sample was converted into CO_2. The reaction was performed at 550°C for 16–18 h. Isotope measurements were made on a Finnigan MAT 252. Oxygen isotope compositions are given in the standard d-notation and expressed relative to VSMOW in permil (‰). The precision of $d^{18}O$ values was better than ±0.2‰, as compared with accepted $d^{18}O$ values for NBS-28 of 9.64‰.

Petrography, Geochemistry and Isotopic Data

Petrographical and geochemical characteristics of the Alaçam granite are given in Hasözbek *et al.* (2011). The pluton includes mainly granites and minor granodiorites. The granite generally exhibits a moderate coarse-grained holocrystalline texture. In places where the margin of the granite is well exposed however, the texture is fine-grained due to rapid cooling (Hasözbek *et al.* 2011). The major mineral assemblage is quartz, albite, orthoclase, hornblende and biotite. Zircon, titanite, apatite, and magnetite are found as accessory minerals (Figure 3). Plagioclases generally exhibit albite twinning and normal oscillatory zoning due to changes in composition from core to rim. The mineral contains small inclusions of hornblende and biotite. Few plagioclases are altered into sericite. Alkali feldspars are mostly microcline or microperthite and may display a cloudy appearance due to sericitization. Most of the quartz minerals exhibit a polygonal structure and vary in size. Generally, amphiboles occur in euhedral-subhedral prismatic or rhombic forms with lamellar twinning (Figure 3a–d).

The granite is subalkaline, high-K calc-alkaline in composition with A/CNK values < 1.1. Ba (288–1330 ppm), La (23–64 ppm), and Th (9–48 ppm) concentrations indicate enrichment in incompatible elements. The chondrite and primordial mantle-normalized element patterns also show enrichment in incompatible elements (Figure 4a, b). High field strength elements such as Pb and low field strength elements such as Rb display negative anomalies (Figure 4b). Negative anomalies in Sr are also significant. Enrichment in LREE ($[La/Yb]_N$= 6–17), as compared to HREE ($[Gd/Yb]_N$ = 1–1.6) is significant in the chondrite-normalized patterns (Hasözbek *et al.* 2011).

Mineral Chemistry

Three identical samples of the Alaçam granite, from margin to centre of the granite, were chosen for Al-in-hornblende barometry evaluations (Figure 2). Results of the microprobe analysis are presented in Table 1. Chemical compositions of the rims and cores of the analyzed amphiboles do not exhibit major compositional differences (Figure 5). Amphiboles are all calcic and range from pargasite to edenite in the calcic-a classification (Figure 5a). In the calcic-b classification diagram of Leake *et al.* (1997), they plot in the magnesiohornblende field (Figure 5b). Fe^{3+}/Fe^{*} ratio ranges from 0.20 to 0.37. The total Al content is between 0.942 and 1.609 cations per formula unit and A-site occupancy ranges from 0.295 to 0.555.

The analytical studies by Hammarstrom & Zen (1986) and Hollister *et al.* (1987) suggested that the Al content of calcic amphibole allowed evaluating the pressure attending to pluton crystallization. Moreover, other experimental studies confirmed an increase in Al content of hornblende with pressure (Schmidt 1992). Pressure calculations for amphibole compositions (rim and core) are given in Table 1. All data fall in the same range between 0.64 and 2.07 kbar. By using a conversion factor of 1 kbar= 3.7 km for continental crust (Tulloch & Challis 2000) and an error factor calculated for the pressure of ±0.5 kbar, the average intrusion depth estimate of the Alaçam granite is 4.7±1.6 km.

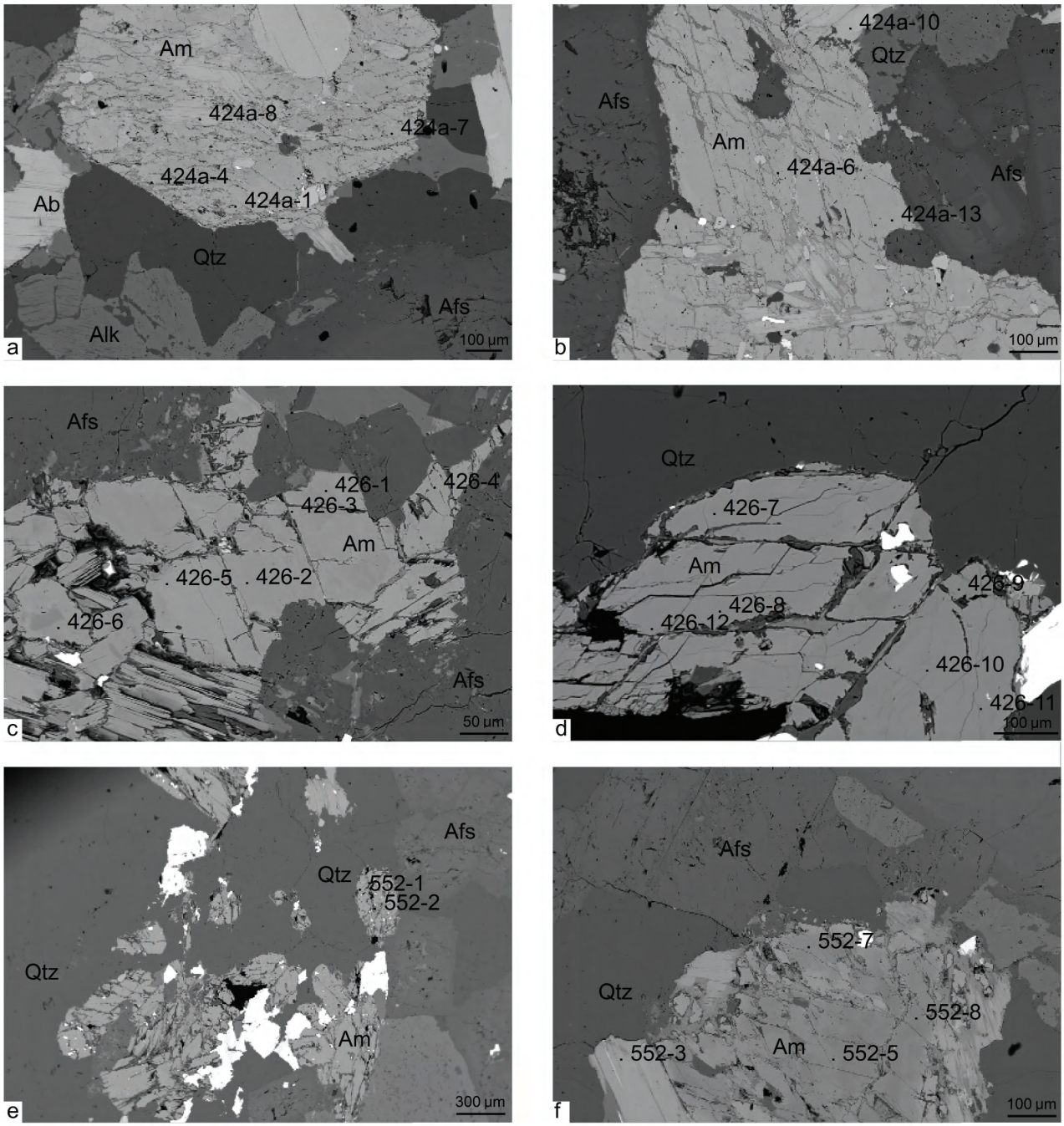

Figure 3. BSE images of mineral textures and spots of microprobe analysis from the Alaçam granite. **(a, b)** 424a, **(c, d)** 426, **(e, f)** 552. Qtz– quartz, Ab– albite, Afs– alkali feldspar, Amamphibole.

Sr-Nd-Pb-O Isotopes

Sr, Nd, Pb, and O isotope analyses are reported in Table 2. Different samples from the Alaçam granite show initial $^{87}Sr/^{86}Sr$ isotopic ratios ranging from 0.70865 to 0.70911. The samples have initial εNd values ranging from –5.3 to –6.3. Initial Pb isotopic composition ranges from 18.87–18.89 for $^{206}Pb/^{204}Pb$, from 15.69–15.70 for $^{207}Pb/^{204}Pb$, and from 38.98–39.00 for $^{208}Pb/^{204}Pb$. $\delta^{18}O$ values of the Alaçam granite range from 9.5 to 10.5 ‰. One sample (550)

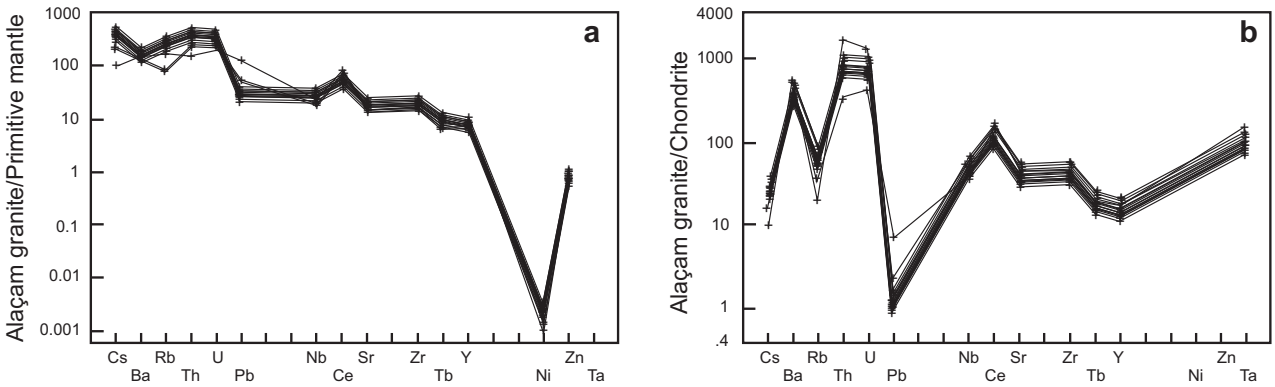

Figure 4. **(a)** Primitive mantle-, **(b)** Chondrite-normalized multielement diagrams for the Alaçam granite. Normalized values are after Taylor & McLennan (1985).

has a $\delta^{18}O$-value of 4.5, which is probably related to isotopic exchange with a low $\delta^{18}O$-fluid at the contact with the granite (Table 2).

Discussion

Emplacement Depths of Aegean and NW Anatolian Granites

Estimates of the emplacement depths of the Aegean and NW Anatolian Miocene granitoids are based on two main lines of evidence: (1) geological features which mainly comprise contact relationships between granitoids and host rocks, occurrence of volcanic counterparts of the pluton, or caldera-type structures (Altunkaynak & Yılmaz 1999; Yılmaz *et al.* 2001; Aydoğan *et al.* 2008; Akay 2009; Hasözbek *et al.* 2010, 2011); (2) geodynamic observations, such as core complexes and syn-extension emplacement structures (Işık & Tekeli 2001; Erkül 2010; Jolivet & Brun 2010; Stouraiti *et al.* 2010). Evidence based on geological features is as follows: the Kozak, Evciler, Kestanbol, Eğrigöz and Koyunoba granitoids crop out with their volcanic counterparts and these granitoids pass gradually into porphyritic volcanic associations which imply a shallow emplacement depth of these granitoids (Karacık & Yılmaz 1998; Altunkaynak & Yılmaz 1998, 1999; Yılmaz *et al.* 2001; Akay 2009). The Eğrigöz and Alaçam granites exhibit wide microgranitic contact zones passing gradually inward into the coarser granitic body that indicates rapid cooling at shallow crustal levels. Rb-Sr biotite ages of 18.8±0.2 Ma from the Eğrigöz granite and 20.01±0.20 Ma from the Alaçam granite are almost concordant with the U-Pb zircon ages, demonstrating rapid cooling after emplacement (Hasözbek *et al.* 2010, 2011). However, roof pendants of the Afyon Zone and the Menderes Massif are exposed in both the Eğrigöz and Koyunoba granites; moreover volcanic counterparts of the granites are intercalated in the granitic bodies (Akay 2009; Hasözbek *et al.* 2010). These features indicate shallow crustal emplacement levels in accordance with the estimate of the emplacement depth of the Alaçam granite.

In many cases, tectonic setting models of the Miocene granites did not properly take into account the emplacement depth of these granites. Most researchers suggested a large-scale crustal extension related emplacement model for these granitoids (i.e., Cyclades Miocene plutonic suites, Eğrigöz, Koyunoba and Alaçam granites in NW Anatolia) (Işık & Tekeli 2001; Bozkurt 2004; Seyitoğlu *et al.* 2004; Jolivet & Brun 2010; Stouraiti *et al.* 2010). The extension model led to a deduction of an intrusion depth between the brittle-ductile transition zones. In general, these types of fault zones can form and evolve in the middle to lower crust (Ramsay 1980; Coward 1984). The location of the transition zone between elastico-frictional (ductile) and quasi-plastic (brittle) behaviour defines an emplacement depth of these granitoids between ca. 15–20 km (Sibson 1977; Brichau *et al.* 2007, 2008; Tirel *et al.* 2009), inconsistent with our new Al-in-hornblende thermobarometry calculations. As mentioned above, geochronological data indicate a rapid cooling of

Table 1. Microprobe analyses of hornblende rims and cores from the Alaçam granite and calculated thermobarometric results.

Sample	**424a-1**	**424a-7**	**424a-8**	**424a-4**	**424a-6**	**424a-10**	**424a-13**	**426-1**	**426-2**	**426-3**	**426-4**	**426-5**	**426-6**	**426-7**	**426-8**	**426-9**	**426-10**	**426-11**	**426-12**	**552-1**	**552-2**	**552-3**	**552-5**	**552-7**	**552-8**
	r	r	c	r/b	c/b	r/b	r	r	c	r	r/b	c/d	c/b	r	c	r	c	r	c	r	r/d	r/b	c	r	c
SiO_2	47.51	45.37	44.7	44.15	44.78	45.26	43.73	45.06	45.34	46.52	46.43	48.44	46.43	44.06	44.05	44.81	44.49	44.58	44.48	45.07	48.16	47.97	49.35	44.33	44.45
TiO_2	0.43	1.245	1.247	1.325	1.086	1.186	1.508	1.483	1.502	0.603	0.586	0.767	0.917	1.72	1.68	1.443	1.425	1.531	1.74	1.304	0.872	0.687	0.625	1.478	1.413
Al_2O_3	6.11	7.99	8.47	8.36	8.11	7.56	9.19	8.11	7.97	6.95	6.88	5.26	6.93	8.84	8.69	8.18	8.55	8.32	8.34	7.95	6.38	5.4	6.7	8.5	8.39
FeO*	20.19	19.49	20.23	20.9	21.32	21.48	21.16	17.87	17.32	18.34	18.19	17.22	18.41	18.87	18.88	18.52	18.87	18.87	19.72	18.01	14.33	17.87	10.57	19.42	19.56
MgO	10.78	10.21	9.55	8.99	9.05	8.59	9.39	10.92	11.54	11.57	11.4	12.46	11.2	10.3	10.14	10.46	10.22	10.49	9.98	11.08	14.38	11.99	16.5	9.97	10.12
MnO	0.979	0.674	0.723	0.851	0.925	1.032	0.678	0.595	0.534	0.785	0.754	0.804	0.841	0.648	0.614	0.711	0.749	0.712	0.737	0.769	0.677	0.983	0.266	0.794	0.743
CaO	10.83	11.12	11.29	11.22	10.88	10.83	11.05	11.4	11.51	11.81	11.93	11.62	11.59	11.39	11.39	11.38	11.29	11.39	11.16	11.19	11.32	11.49	11.73	11.13	11.19
Na_2O	1.233	1.77	1.76	1.72	1.77	1.58	1.86	1.59	1.68	1.154	1.245	1.034	1.235	1.74	1.7	1.58	1.65	1.51	1.64	1.72	1.56	1.285	1.66	1.72	1.79
K_2O	0.533	0.882	1.003	1.024	0.894	0.823	1.018	0.937	0.922	0.633	0.638	0.499	0.756	1.054	1.082	0.97	1.025	0.992	0.913	0.881	0.539	0.518	0.485	1.012	0.944
F	0.102	0.133	0.162	0.161	0.155	0.164	0.144	0.152	0.135	0.067	0.068	0.064	0.075	0.165	0.185	0.149	0.153	0.154	0.13	0.147	0.05	0.049	0.041	0.16	0.149
Cl	0.224	0.334	0.276	0.32	0.342	0.247	0.35	0.214	0.223	0.17	0.202	0.17	0.19	0.2	0.183	0.155	0.165	0.18	0.149	0.32	0.365	0.259	0.458	0.274	0.274
Sum	98.92	96.10	99.41	99.02	99.31	98.75	100.0	98.33	96.10	98.60	98.32	98.34	98.57	98.99	98.59	98.36	98.59	98.73	98.99	98.44	96.10	98.50	98.39	98.79	99.02
Fe_2O_3,calc	5.93	4.65	4.51	4.73	5.37	4.75	6.31	4.25	4.36	6.56	6.03	3.89	5.68	4.71	4.28	4.45	4.66	5.39	5.17	5.05	4.49	3.55	4.32	4.90	5.20
FeO,calc	14.86	15.30	16.17	16.65	16.49	17.21	15.49	14.04	13.40	12.44	12.77	13.72	13.30	14.63	15.03	14.52	14.68	14.02	15.07	13.46	10.29	14.68	6.68	15.01	14.88
H_2O,calc	1.89	1.85	1.84	1.81	1.82	1.83	1.83	1.87	1.88	1.93	1.91	1.94	1.92	1.86	1.85	1.88	1.87	1.87	1.89	1.84	1.93	1.92	1.95	1.83	1.84
O= F, Cl	0.09	0.13	0.13	0.14	0.14	0.12	0.14	0.11	0.11	0.07	0.07	0.07	0.07	0.11	0.12	0.10	0.10	0.11	0.09	0.13	0.10	0.08	0.12	0.13	0.12
SUM	101.32	101.4	101.5	101.1	101.5	100.3	102.4	100.5	100.8	101.1	100.7	100.6	100.9	101.2	100.7	100.5	100.8	101.0	101.3	100.6	100.9	100.7	100.6	100.9	101.2
Fe^3/Fe^*	**0.26**	**0.21**	**0.20**	**0.20**	**0.23**	**0.20**	**0.27**	**0.21**	**0.23**	**0.32**	**0.30**	**0.20**	**0.28**	**0.22**	**0.20**	**0.22**	**0.22**	**0.26**	**0.24**	**0.25**	**0.28**	**0.18**	**0.37**	**0.23**	**0.24**
Formula per Holland & Blundy 1994																									
T-sites																									
Si	7.022	6.742	6.669	6.646	6.705	6.814	6.493	6.714	6.712	6.853	6.871	7.132	6.866	6.565	6.597	6.694	6.645	6.635	6.626	6.709	6.985	7.100	7.039	6.631	6.629
Al_{iv}	0.978	1.258	1.331	1.354	1.295	1.186	1.507	1.286	1.288	1.147	1.129	0.868	1.134	1.435	1.403	1.306	1.355	1.365	1.374	1.291	1.015	0.900	0.961	1.369	1.371
$Al_{(total)}$	1.065	1.400	1.490	1.484	1.432	1.342	1.609	1.425	1.391	1.207	1.200	0.913	1.208	1.553	1.534	1.441	1.505	1.460	1.465	1.395	1.091	0.942	1.127	1.499	1.475
M1,2,3 sites																									
Alvi	0.086	0.142	0.159	0.129	0.137	0.156	0.101	0.138	0.103	0.060	0.072	0.045	0.074	0.118	0.132	0.135	0.150	0.095	0.091	0.104	0.076	0.042	0.165	0.129	0.104
Ti	0.048	0.139	0.140	0.150	0.122	0.134	0.168	0.166	0.167	0.067	0.065	0.085	0.102	0.193	0.189	0.162	0.160	0.171	0.195	0.146	0.095	0.076	0.067	0.166	0.158
Fe^{3+}	0.659	0.520	0.506	0.535	0.605	0.538	0.704	0.477	0.486	0.727	0.671	0.431	0.632	0.528	0.482	0.500	0.524	0.604	0.579	0.566	0.490	0.395	0.464	0.552	0.584
Mg	2.374	2.261	2.123	2.017	2.020	1.927	2.078	2.425	2.546	2.540	2.514	2.734	2.468	2.287	2.263	2.329	2.275	2.327	2.216	2.458	3.108	2.645	3.507	2.222	2.249
Mn	0.123	0.085	0.091	0.109	0.117	0.132	0.085	0.075	0.067	0.098	0.095	0.100	0.105	0.082	0.078	0.090	0.095	0.090	0.093	0.097	0.083	0.123	0.032	0.101	0.094

Table 1. (Contunied).

Fe^{2+}	1.710	1.852	1.980	2.060	1.999	2.112	1.863	1.719	1.631	1.508	1.580	1.606	1.618	1.792	1.856	1.784	1.796	1.712	1.826	1.628	1.147	1.718	0.764	1.829	1.810
Ca	0.000	0.000	0.000	0.000	0.000	0.000	0.000	0.000	0.000	0.000	0.003	0.000	0.000	0.000	0.000	0.000	0.000	0.000	0.000	0.000	0.000	0.000	0.000	0.000	0.000
	5.000	5.000	5.000	5.000	5.000	5.000	5.000	5.000	5.000	5.000	5.000	5.000	5.000	5.000	5.000	5.000	5.000	5.000	5.000	5.000	5.000	5.000	5.000	5.000	5.000
M4 site																									
Fe	0.127	0.049	0.038	0.036	0.066	0.054	0.060	0.031	0.028	0.025	0.000	0.084	0.027	0.032	0.027	0.030	0.037	0.032	0.052	0.047	0.101	0.099	0.033	0.048	0.046
Ca	1.715	1.771	1.805	1.810	1.746	1.747	1.758	1.820	1.826	1.864	1.889	1.833	1.836	1.819	1.828	1.822	1.807	1.817	1.781	1.785	1.759	1.822	1.793	1.784	1.788
Na	0.158	0.180	0.157	0.155	0.188	0.198	0.182	0.149	0.146	0.111	0.111	0.083	0.137	0.150	0.145	0.148	0.156	0.151	0.167	0.168	0.140	0.079	0.175	0.168	0.166
	2.000	2.000	2.000	2.000	2.000	2.000	2.000	2.000	2.000	2.000	2.000	2.000	2.000	2.000	2.000	2.000	2.000	2.000	2.000	2.000	2.000	2.000	2.000	2.000	2.000
A site																									
Ca	0.000	0.000	0.000	0.000	0.000	0.000	0.000	0.000	0.000	0.000	0.000	0.000	0.000	0.000	0.000	0.000	0.000	0.000	0.000	0.000	0.000	0.000	0.000	0.000	0.000
Na	0.195	0.330	0.352	0.347	0.326	0.263	0.354	0.310	0.336	0.218	0.246	0.212	0.217	0.353	0.349	0.309	0.322	0.285	0.307	0.329	0.299	0.290	0.284	0.331	0.352
K	0.100	0.167	0.191	0.197	0.171	0.158	0.193	0.178	0.174	0.119	0.120	0.094	0.143	0.200	0.207	0.185	0.195	0.188	0.174	0.167	0.100	0.098	0.088	0.193	0.180
Sum A	0.295	0.497	0.543	0.544	0.496	0.421	0.546	0.488	0.510	0.337	0.367	0.306	0.360	0.553	0.555	0.494	0.517	0.473	0.480	0.496	0.399	0.388	0.373	0.524	0.531
OH site																									
O	0.000	0.000	0.000	0.000	0.000	0.000	0.000	0.000	0.000	0.000	0.000	0.000	0.000	0.000	0.000	0.000	0.000	0.000	0.000	0.000	0.000	0.000	0.000	0.000	0.000
OH	1.895	1.852	1.852	1.840	1.838	1.857	1.842	1.873	1.880	1.925	1.916	1.927	1.916	1.870	1.865	1.889	1.885	1.881	1.900	1.848	1.886	1.911	1.869	1.853	1.859
F	0.048	0.063	0.077	0.078	0.074	0.079	0.069	0.072	0.064	0.032	0.032	0.030	0.036	0.079	0.089	0.071	0.073	0.073	0.062	0.070	0.023	0.023	0.019	0.077	0.071
Cl	0.057	0.085	0.071	0.083	0.088	0.064	0.089	0.055	0.057	0.043	0.051	0.043	0.048	0.051	0.047	0.040	0.042	0.046	0.038	0.082	0.091	0.066	0.112	0.070	0.070
	2.000	2.000	2.000	2.000	2.000	2.000	2.000	2.000	2.000	2.000	2.000	2.000	2.000	2.000	2.000	2.000	2.000	2.000	2.000	2.000	2.000	2.000	2.000	2.000	2.000
Sum cations	15.29	15.49	15.54	15.54	15.49	15.42	15.54	15.48	15.51	15.33	15.36	15.30	15.36	15.55	15.55	15.49	15.51	15.47	15.48	15.49	15.39	15.38	15.37	15.52	15.53
Mg/Fe^{2+}	1.293	1.189	1.052	0.962	0.978	0.890	1.080	1.386	1.535	1.657	1.591	1.618	1.501	1.254	1.202	1.284	1.241	1.334	1.180	1.467	2.490	1.456	4.400	1.184	1.212
Thermobarometric results																									
Ps (kb)	2.06	3.65	4.08	4.05	3.80	3.38	4.65	3.77	3.61	2.74	2.70	1.34	2.74	4.38	4.29	3.85	4.16	3.94	3.96	3.63	2.18	1.48	2.35	4.12	4.01
Anderson & Smith (pressure at various thermometers)																									
T (C) HB1*	770.2	817.3	825.6	849.6	827.5	783.7	923.9	844.0	877.3	840.8	840.0	791.7	824.1	916.5	890.7	849.8	854.5	886.4	904.6	859.2	814.4	805.9	758.5	859.8	887.6
P(Kb) HB1*	0.86	1.15	1.27	0.54	1.00	1.73	-1.71	0.49	-0.69	-0.23	-0.23	-0.18	0.23	-1.59	-0.67	0.37	0.46	-0.77	-1.42	-0.09	0.02	-0.36	1.33	0.27	-0.76
T (C) HB2	**773.2**	**800.3**	**794.9**	**804.2**	**809.0**	**789.0**	**841.4**	**806.5**	**818.2**	**786.4**	**782.4**	**747.1**	**796.3**	**832.0**	**821.6**	**808.9**	**814.5**	**826.1**	**838.9**	**817.4**	**787.1**	**744.0**	**764.1**	**818.0**	**826.7**
P(Kb) HB2	**0.80**	**1.58**	**2.07**	**1.82**	**1.49**	**1.62**	**1.25**	**1.52**	**1.09**	**1.12**	**1.18**	**0.60**	**0.91**	**1.33**	**1.55**	**1.53**	**1.63**	**1.14**	**0.79**	**1.13**	**0.64**	**0.77**	**1.23**	**1.51**	**1.18**
T (C) BH	728.0	786.9	804.4	813.8	796.8	768.1	866.3	823.9	827.9	791.7	785.9	725.5	787.0	878.1	863.9	830.2	844.8	854.2	857.9	810.1	744.4	721.7	725.6	830.7	833.7
P(Kb) BH	1.53	1.90	1.84	1.57	1.79	2.06	0.45	1.07	0.83	1.01	1.11	0.89	1.11	-0.15	0.26	0.95	0.77	0.31	0.21	1.32	1.41	1.07	1.84	1.16	0.98

HB 1 refers to Holland & Blundy (1990) Hbld-Plag thermometry calibration reaction edenite + 4 quartz= tremolite + albite, HB 2 refers to Holland & Blundy (1990). Hbld-Plag thermometry calibration reaction edenite + albite = richterite + anorthite, BH refers to Blundy & Holland (1994). Hbld-Plag thermometry calibration reaction edenite + 4 quartz= tremolite + albite. Pressure by Schmidt (1992) (Ps), and Anderson & Smith, (1995). Cations based on 23O and summed to 13. r– rim, c– core, b– bright, d– dark.

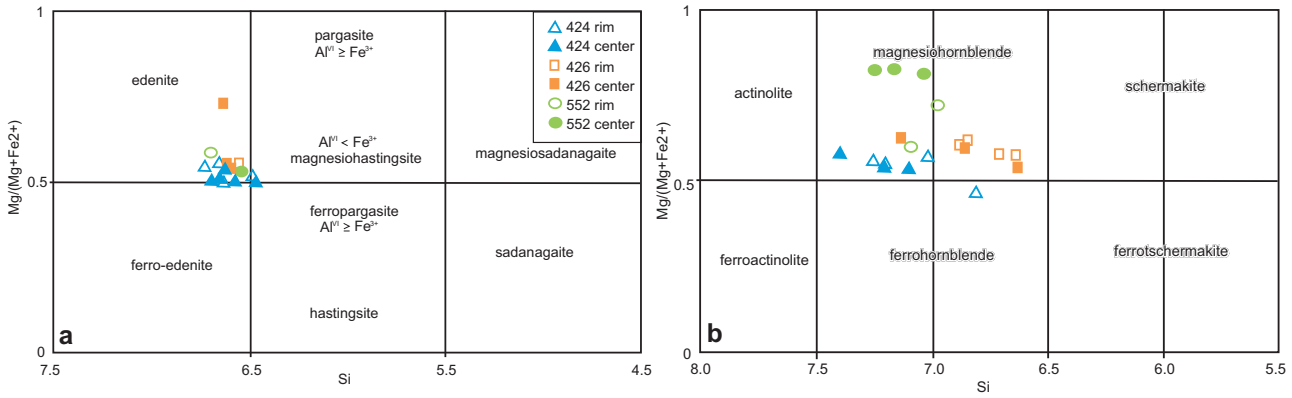

Figure 5. Amphibole classification diagrams of Leake *et al.* (1997) for the Alaçam granite based on **(a)** calcic-a, and **(b)** calcic- b.

Table 2. Sr-Nd-Pb-O isotope composition of whole-rock samples from the Alaçam granite.

ALAÇAM GRANITE

Sample	Sr(ppm)	Rb(ppm)	$^{87}Rb/^{86}Sr$	$^{87}Sr/^{86}Sr$	$^{87}Sr/^{86}Sr(i)$	Sm(ppm)	Nd(ppm)	$^{147}Sm/^{144}Nd$	$^{143}Nd/^{144}Nd$	$^{143}Nd/^{144}Nd$ (i)	eNd	$^{206}Pb/^{204}Pb$	$^{207}Pb/^{204}Pb$	$^{208}Pb/^{204}Pb$	$\delta^{18}O_{SMOW}$
550	254	163.8	1.866	0.70963	0.70910	4.69	25.4	0.1121	0.51234	0.51233	-5.8	18.873	15.7	39.003	4.5
620	261	188.9	2.094	0.70974	0.70915	5.48	29.4	0.1132	0.51237	0.51235	-5.3	18.89	15.696	38.988	9.5
189	343.5	145.3	1.224	0.70900	0.70865	5.3	31	0.1038	0.51234	0.51233	-5.8	18.896	15.71	39.002	10.5
1045	309.9	124.1	1.159	0.70939	0.70906	6.4	36.2	0.1073	0.51232	0.51231	-6.2	18.902	15.699	39.017	10.3
859	316.6	135.4	1.238	0.70931	0.70895	4.9	23.7	0.1255	0.51231	0.5123	-6.4	18.891	15.698	39.007	10.3
505	260	164	1.825	0.70963	0.70911	5.33	30.3	0.1068	0.51234	0.51233	-5.8	18.879	15.702	38.997	9.9

Sr, Rb, Sm, Nd concentrations are in ppm. (i): initial. SMOW: Standard Mean Ocean Water. Pb is corrected by 0.8‰ mass unit

the granitic body on account of close consistency between the U-Pb zircon age (20.0±1.4 Ma) and Rb-Sr biotite age (20.01±0.20 Ma) (Hasözbek *et al.* 2011). Al-in-hornblende barometry evaluations were also performed on the Çavuşlu and Eybek plutons in NW Anatolia (Ghassab 1994) and resulting emplacement depth calculations are 8.7±2.2 km, 7.2±2.2 km respectively, indicating shallow emplacement levels. On a regional scale, i.e., from east to west along the northern and southern parts of the İzmir-Ankara Suture Zone, emplacement depths of the Miocene granitoids increases, but never reaches the depth of the transition zone between elastico-frictional (ductile) and quasi-plastic (brittle) where low-angle extension-related mechanisms might be triggered. Therefore, the emplacement depth estimates of the Miocene granites greatly limit the crustal-scale extension model which requires deep-seated melt injections at about 15–20 km (Brichau *et al.* 2007, 2008) into the footwall of a regional detachment fault.

Isotopic Compositions of the Alaçam Granite

Miocene granites of NW Anatolia are mostly peraluminous or slightly metaluminous I-type granitoids (Altunkaynak & Yılmaz 1999; Yılmaz *et al.* 2001; Aydoğan *et al.* 2008; Akay 2009; Hasözbek *et al.* 2010, 2011). In NW Anatolia, S-type characteristics are mostly seen in the basement crystalline rocks such as gneisses of the Menderes Massif and the Afyon Zone (Hasözbek *et al.* 2010). In the southern Aegean Sea, previous studies on both I-and S-type Miocene granitoids indicate a heterogeneous metasedimentary crustal source rather than mantle components (Stouraiti *et al.* 2010). Granite generation, including in the Eastern Mediterranean area, is still hotly

debated, due to the complex geodynamic features and crustal rheology in such areas. However, previous studies in the Aegean Sea seem to confirm that the granitoids are derived from a crustal metasedimentary source (Altherr & Siebel 2002; Stouraiti *et al.* 2010). Stouraiti *et al.* (2010) inferred the granites to be derived from metasedimentary biotite-gneiss, marble, and amphibolites. In NW Anatolia, only a few studies addressed the generation of the Miocene granites (Aldanmaz *et al.* 2000; Dilek & Altunkaynak 2007, 2009; Aydoğan *et al.* 2008). These researchers suggested a contribution of mantle material related to slab-break off was involved during magma generation. Aydoğan *et al.* (2008) claimed that both mantle and crustal contributions were responsible for the generation of Miocene magmatism in the Uşak area (Baklan granite).

Initial $^{87}Sr/^{86}Sr$ versus Rb/Sr and initial $^{87}Sr/^{86}Sr$ versus 1000/Sr diagrams show samples of the Alaçam granite exhibiting a positive trend, which clearly implies that crustal assimilation played an important role rather than a fractional crystallization during the evolution of this granite (Figure 6a, b). Pb isotopic compositions of the Alaçam granite plot close to the EMII field in $^{208}Pb/^{204}Pb$ versus $^{206}Pb/^{204}Pb$, $^{207}Pb/^{204}Pb$ versus $^{206}Pb/^{204}Pb$, and $^{87}Sr/^{86}$ Sr versus $^{206}Pb/^{204}Pb$ plots (Table 2, Figure 7), which also corresponds to middle continental crust composition (Rudnick & Goldstein 1990).

The Alaçam granite displays lower initial $^{87}Sr/^{86}Sr$ and $\delta^{18}O$ values than average S-type granitoids (Table 2, Figure 8). Besides, typical examples of the S-type granites on Aegean Islands (Tinos and Ikeria) show considerably higher Sr-O ratios (Altherr *et al.* 1998) than samples from the Alaçam granite (Figure 8). Isotopic compositions of the Alaçam granite plot between those of I-type and S-type granites in general; however all other petrographical and geochemical data support the I-type nature of this granite as commonly seen in other Miocene granites in NW Anatolia (Karacık & Yılmaz 1998; Altunkaynak & Yılmaz 1999; Yılmaz *et al.* 2001; Akay 2009; Hasözbek *et al.* 2010, 2011). I- and S-type notation usually implies that the rocks derived from pure igneous or sedimentary sources. However, this can easily be misleading because these are end-member types and many granites are likely to have a mixed source or undergone some contamination during their formation (Chen & Grapes 2007).

In Figure 9 samples of the Alaçam granite are plotted in the $e_{Nd(i)}$ versus $^{87}Sr/^{86}Sr_{(i)}$ diagram together with representative samples from Miocene granitoids of the central Aegean (Ikera, Tinos) and metasedimentary rocks from Aegean islands and the Menderes Massif. The Alaçam granite has a distinct middle crust signature compared to the Aegean islands granitoids (Ikera, Tinos). Besides, all granite samples from NW Anatolia and the Aegean islands plot in the crustal field. Moreover, Sr-Nd-O isotopic constraints support an older crustal source (Menderes Massif) for the Alaçam granite, rather than a mantle contribution which was also previously envisaged for the Aegean Miocene granitoids (Juteau *et al.* 1986; Dilek & Altunkaynak 2007). Additional evidence

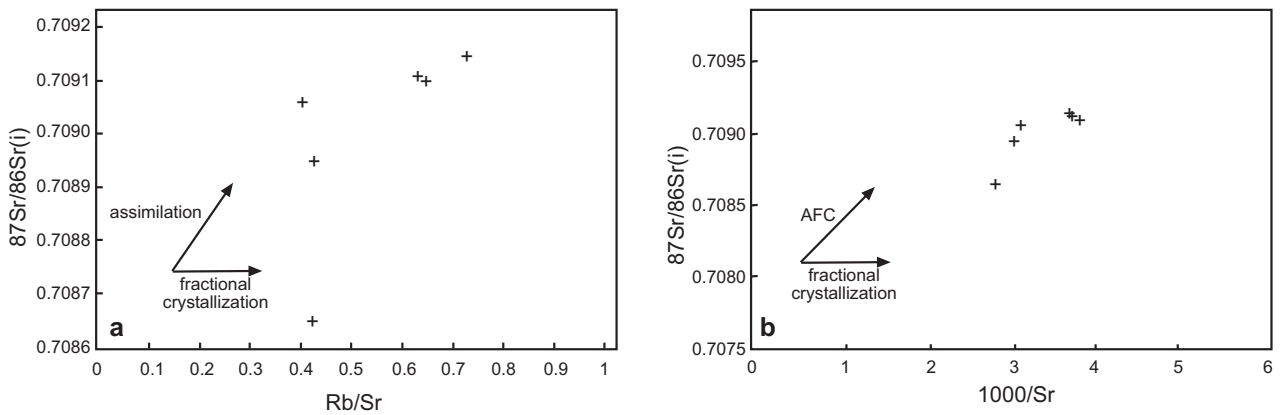

Figure 6. **(a)** Initial $^{87}Sr/^{86}Sr$ vs Rb/Sr, **(b)** Initial $^{87}Sr/^{86}Sr$ vs 1000/Sr ratios for the Alaçam granite (see Table 2) implying assimilation rather than fractional crystallization during magma genesis.

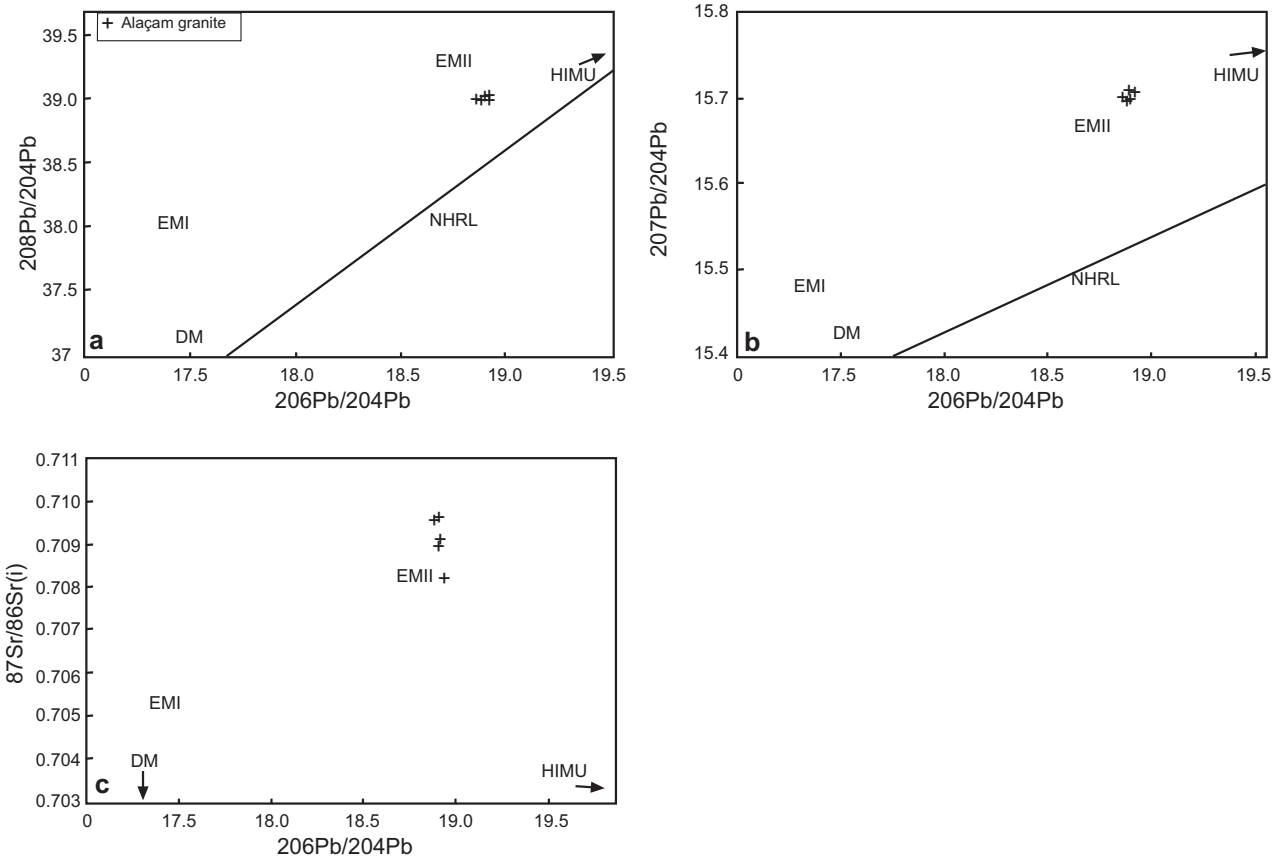

Figure 7. **(a)** $^{208}Pb/^{204}Pb$ vs $^{206}Pb/^{204}Pb$, **(b)** $^{207}Pb/^{204}Pb$ vs $^{206}Pb/^{204}Pb$, **(c)** initial $^{87}Sr/^{86}Sr$ vs $^{206}Pb/^{204}Pb$ ratios for the Alaçam granite. EM– Enriched Mantle, DP– Depleted Mantle, NHRL– Northern Hemisphere Reference Line, HIMU– high-μ (Hart 1984, 1988; Hart *et al.* 1986).

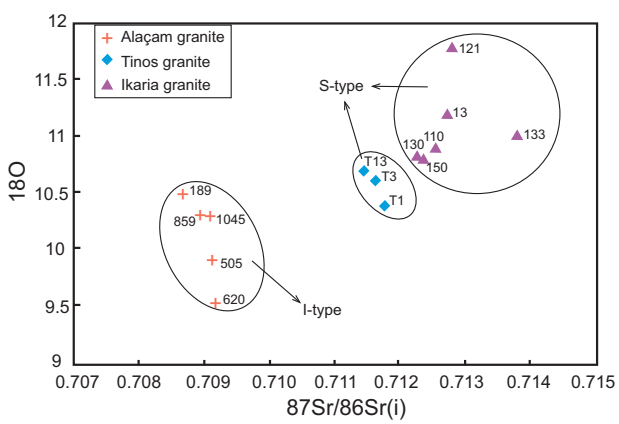

Figure 8. Whole rock $\delta^{18}O$ versus initial $^{87}Sr/^{86}Sr$ of the Alaçam granite (this study), Ikaria and Tinos granites (Altherr *et al.* 1998) showing the I-type and S-type granites in the Aegean Islands and NW Anatolia (Alaçam granite).

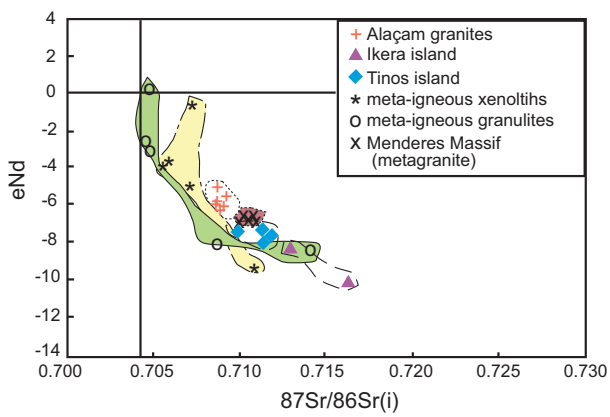

Figure 9. $e_{Nd}(I)$ versus $^{87}Sr/^{86}Sr_{(i)}$ ratios for the Alaçam granite (see Table 2) and various Miocene granitoids (Tinos, Ikaria) (Stouraiti *et al.* 2010) from the Aegean islands and basement rocks of the Menderes Massif (metagranite) (Hasözbek *et al.* 2010).

for an older crustal source can be gained from the U-Pb zircon upper intercept 550–500 Ma ages of the Alaçam granite (Hasözbek *et al.* 2010, 2011). A distinctive pattern is observed for Pb isotopes of the Alaçam granite (Table 2, Figure 7). In $^{208}Pb/^{204}Pb$ versus $^{206}Pb/^{204}Pb$, $^{207}Pb/^{204}Pb$ versus $^{206}Pb/^{204}Pb$, and $^{87}Sr/^{86}$ Sr versus $^{206}Pb/^{204}Pb$ plots (Figures 7a–c) the Alaçam granite exhibits higher Pb isotope ratios, supporting a dominantly crustal contribution during melt formation (Wilson 1989).

Conclusions

Based on new Al-in-hornblende barometry and isotopic data the following conclusions about the Alaçam granite can be drawn:

1. The estimated emplacement depth for the Alaçam granite is 4.7±1.6 km. A shallow crustal emplacement is compatible with geological and geochronological data in the area. A previously challenged syn-extension (low-angle fault) related emplacement of the Alaçam granite along a ductile-brittle transition zone (ca. 15–20 km) is not consistent within this emplacement depth estimate. Estimated emplacement depths of other Miocene granites in NW Anatolia limit the validity of the syn-extension emplacement model along the northern part of the Menderes Massif.
2. The emplacement depths of the Miocene granites increase from east to west, but even maximum values are insufficient to trigger the low-angle extensional type of emplacement.
3. Sr-Nd-Pb-O isotopic compositions of the Alaçam granite are consistent with derivation from a middle crustal source rather than a mantle source. Isotopic data are also compatible with dehydration melting of metaluminous older crustal sources, as previously suggested for eastern Mediterranean magmatism by Stouraiti *et al.* (2010).

Acknowledgements

This study was financially supported by the DAAD, Scientific and Technological Research Council of Turkey (TÜBİTAK) and Dokuz Eylül University, Scientific Research Projects Foundation (project no: 2009. KB. FEN. 074). A. Okay, O. Candan, E. Koralay, G. Topuz, E.V. Muratçay and C. Pin are thanked for help and discussion. T. Wenzel, Institute of Geosciences, Tübingen is thanked for support during microprobe analyses. E. Reitter, Department of Geochemistry, Tübingen University, is thanked for technical help.

References

Akal, C. 2003. Mineralogy and geochemistry of melilite leucitites, Balıkesir, Afyon (Turkey). *Turkish Journal of Earth Sciences* **12**, 215–239.

Akay, E. 2009. Geology and petrology of the Simav Magmatic Complex (NW Anatolia) and its comparison with the Oligo–Miocene granitoids in NW Anatolia: implications on Tertiary tectonic evolution of the region. *International Journal of Earth Sciences* **98**, 1655–1675.

Aldanmaz, E., Pearce, J., Thirlwall, M.F. & Mitchell, J. 2000. Petrogenetic evolution of late Cenozoic, post-collision volcanism in western Anatolia, Turkey. *Journal of Volcanology and Geothermal Research* **102**, 67–95.

Altherr, R., Henjes-Kunst, F., Matthews, A., Friedrichsen, H. & Hansen, B.T. 1998. O-Sr isotopic variations in Miocene granitoids from the Aegean: evidence for an origin by combined assimilation and fractional crystallization. *Contributions to Mineralogy and Petrology* **100**, 528–541.

Altherr, R. & Siebel, W. 2002. I-type plutonism in a continental back-arc setting: Miocene granitoids and monzonites from the central Aegean Sea, Greece. *Contributions to Mineralogy and Petrology* **143**, 397–415.

Altherr, R., Topuz, G., Marschall, H., Zack, T. & Ludwig, T. 2004. Evolution of a tourmaline-bearing lawsonite eclogite from the Elekdağ area (Central Pontides, N Turkey): evidence for infiltration of slab-derived B-rich fluids during exhumation. *Contributions to Mineralogy and Petrology* **148**, 409–425.

Altunkaynak, S. 2007. Collision-driven slab breakoff magmatism in northwestern Anatolia, Turkey. *Journal of Geology* **115**, 63–82.

Altunkaynak, S. & Yilmaz, Y. 1998. The Mount Kozak magmatic complex, western Anatolia. *Journal of Volcanology and Geothermal Research* **85**, 211–231.

Altunkaynak, S. & Yilmaz, Y. 1999. The Kozak Pluton and its emplacement. *Geological Journal* **34**, 257–274.

Anderson, J.L. & Smith, D.R. 1995. The effect of temperature and oxygen fugacity on Al-in-hornblende barometry. *American Mineralogist* **80**, 549–559.

Armstrong, J.T. 1991. Quantitative elemental analysis of individual microparticles with electron beam instruments. *In*: Heinrich, K.F.J. & Newbury, D.E. (eds), *Electron Probe Quantitation*. Plenum, New York, 261–315.

Aydoğan, M.S., Çoban, H., Bozcu, M. & Akinci, O. 2008. Geochemical and mantle-like isotopic (Nd, Sr) composition of the Baklan Granite from the Muratdağı Region (Banaz, Uşak), western Turkey: implications for input of juvenile magmas in the source domains of western Anatolia Eocene–Miocene granites. *Journal of Asian Earth Sciences* **33**, 155–176.

Beccaluva, L., Di Girolamo, P. & Serri, G. 1991. Petrogenesis and tectonic setting of the Roman volcanic province, Italy. *Lithos* **26**, 1991–221.

Blundy, J.D. & Holland, T.J.B. 1990. Calcic amphibole equilibria and a new amphibole-plagioclase geothermometer. *Contributions to Mineralogy and Petrology* **104**, 208–224.

Bozkurt, E. 2004. Granitoid rocks of the southern Menderes Massif (southwestern Turkey): field evidence for Tertiary magmatism in an extensional shear zone. *International Journal of Earth Sciences* **93**, 52–71.

Bozkurt, E. & Oberhänsli, R. 2001. Menderes Massif (Western Turkey): structural, metamorphic and magmatic evolution – a synthesis. *International Journal of Earth Sciences* **89**, 679–708.

Brichau, S., Ring, U., Carter, A., Monie, P., Bolhar, R., Stockli, D. & Brunel, M. 2007. Extensional faulting on Tinos island, Aegean sea, Greece: How many detachments? *Tectonics* **26**, 4–16.

Brichau, S., Ring, U., Carter, A., Bolhar, R., Monie, P., Stockli, D. & Brunel, M. 2008. Timing, slip rate, displacement and cooling history of the Mykonos detachment footwall, Cyclades, Greece, and implications for the opening of the Aegean Sea basin. *Journal of the Geological Society, London* **165**, 263–277.

Candan, O., Çetİnkaplan, M., Oberhänsli, R., Rimmele, G. & Akal, C. 2005. Alpine high-P/low-T metamorphism of the Afyon Zone and implications for the metamorphic evolution of Western Anatolia, Turkey. *Lithos* **84**, 102–124.

Chen, N.G. & Grapes, R. 2007. *Granite Genesis: In-situ Melting and Crustal Evolution*. Springer, Dordrecht, Netherlands.

Clayton, R.N. & Mayeda, T.K. 1963. The use of bromine pentafluoride in the extraction of oxygen from oxides and silicates for isotopic analysis. *Geochemica Cosmochimica Acta* **27**, 43–52.

Coward, M.P. 1984. Precambrian crust: examples from NW Scotland and southern Africa and their significance. *In*: Kröner, A. & Greiling, R. (eds), *Precambrian Tectonics Illustrated*. Stuttgart, e., Schweizerbartische Verlangsbuchhandlung (Nägele u. Obermiller), 207–235.

Dilek, Y. & Altunkaynak, S. 2007. Cenozoic crustal evolution and mantle dynamics of post-collisional magmatism in western Anatolia. *International Geology Review* **49**, 431–453.

Dilek, Y. & Altunkaynak, S. 2009. Geochemical and temporal evolution of Cenozoic magmatism in western Turkey: mantle response to collision, slab breakoff, and lithospheric tearing in an orogenic belt. *In:* Van Hinsbergen, D.J.J., Edwards, M.A. & Govers, R. (eds), *Collision and Collapse at the Africa–Arabia–Eurasia Subduction Zone*. Geological Society London, Special Publications **311**, 213–234.

Erkül, F. 2010. Tectonic significance of synextensional ductile shear zones within the Early Miocene Alaçam granites, Northwestern Turkey. *Geological Magazine* **147**, 611–637.

Ghassab, T.R. 1994. *Alpidsche Entwicklunsgechichte des Kazdag Massivs und der angrenzenden Granitoide (Biga Halbinsel, NW-Türkei): Eine geologische, geochemische und geochronologische Studie*. Diplomarbeit, Tübingen University [in German, unpublished].

Güngör, T. & Erdoğan, B. 2001. Emplacement age and direction of the Lycian Nappes in the Söke-Selçuk region, western Turkey. *International Journal of Earth Sciences* **89**, 874–882.

Güngör, T. & Erdoğan, B. 2002. Tectonic significance of mafic volcanic rocks in a Mesozoic sequence of the Menderes Massif, West Turkey, *International Journal of Earth Sciences* **91**, 386–397.

Hammarstrom, J.A. & Zen, E.A. 1986. Aluminium in hornblende: an emprical igneous geobarometer. *American Mineralogist* **71**, 1297–1313.

Hart, S.R. 1984. A large-scale isotope anomaly in the Southern Hemisphere mantle. *Nature* **309**, 753–757.

Hart, S.R. 1988. Heterogeneous mantle domains: signatures, genesis and mixing chronologies. *Earth and Planetary Science Letters* **90**, 273–296.

Hart, S.R., Gerlach, D.C. & White, W.M. 1986. A possible new Sr-Nd-Pb mantle array and consequences for mantle mixing. *Geochimica Cosmochimica Acta* **50**, 1551–1557.

Hasözbek, A., Akay, E., Erdoğan, B., Satir, M. & Siebel, W. 2010. Early Miocene granite formation by detachment tectonics or not? A case study from the northern Menderes Massif (Western Turkey). *Journal of Geodynamics* **50,** 67–80.

Hasözbek, A., Satir, M., Erdoğan, B., Akay, E. & Siebel, W. 2011. Early Miocene post-collisional magmatism in NW Turkey: geochemical and geochronological constraints. *International Geology Review* 53, 1098–1119.

Holland, T. & Blundy, J. 1994. Non-ideal interactions in calcic amphiboles and their bearing on amphibole-plagioclase thermometry. *Contribution in Mineralogy and Petrology* **116**, 433–47.

Hollister, L.S., Grissom, G.C., Peters, E.K., Stowell, H.H. & Sisson, V.B. 1987. Confirmation of the emprical correlation of Al in hornblende with pressure of solidification of calc-alkaline plutons. *American Mineralogist* **72**, 231–239.

İlbeyli, N. & Kibici, Y. 2009. Collision-related granite magma genesis, potential sources and tectono-magmatic evolution: comparison between central, northwestern and western Anatolia (Turkey). *International Geology Review* **51**, 252–278.

Işık, V., Seyitoğlu, G. & Çemen, İ. 2003. Ductile-brittle transition along the Alaşehir detachment fault and its structural relationship with the Simav detachment fault, Menderes Massif, western Turkey. *Tectonophysics* **374**, 1–18.

Işık, V. & Tekeli, O. 2001. Late orogenic crustal extension in the northern Menderes Massif (western Turkey): evidence for metamorphic core complex formation. *International Journal of Earth Sciences* **89**, 757–765.

Jolivet, L. & Brun, J.P. 2010. Cenozoic geodynamic evolution of the Aegean. *International Journal of Earth Sciences* **99**, 109–138.

Juteau, M., Michard, A. & Albarede, F. 1986. The Pb-Sr-Nd isotope geochemistry of some recent circum-Mediterranean granites. *Contributions to Mineralogy and Petrology* **92**, 331–340.

Karacik, Z. & Yilmaz, Y. 1998. Geology of the ignimbrites and the associated volcano plutonic complex of the Ezine area, northwestern Anatolia. *Journal of Volcanology and Geothermal Research* **85**, 251–264.

Leake, B.E., Woolley, A.R., Arps, C.E.S., Birch, W.D., Gibert, M.C., Grice, J.D., Hawthorne, F.C., Kato, A., Kisch, H.J., Krivovichev, V.G., Linthout, K., Laird, J., Mandarino, J., Maresch, W.V., Nickel, E.H., Rock, N.M.S., Schumacher, J.C., Stephenson, N.C.N., Whittaker, E.J.W. & Youzhi, G. 1997. Nomenclature of amphiboles: report of the Subcommittee on Amphiboles of the International Mineralogical Association Commission on New Minerals and Mineral Names. *Mineralogical Magazine* **61**, 295–321.

Neubauer, F. & Raumer, J.V. 1993. The Alpine basement-linkage between Variscidesand east-Mediterranean mountain belt. *In*: Raumer, J.F. & Neubauer, F. (eds), *Pre-Mesozoic Geology in the Alps.* Springer-Verlag, 641–664.

Okay, A.I. 1980. Lawsonite zone blueschists and a sodic amphibole producing reaction in the Tavşanlı region, Northwest Turkey. *Contributions to Mineralogy and Petrology* **75**, 179–186.

Okay, A.I. 1982. Incipient blueschist metamorphism and metasomatism in the Tavşanlı region, Northwest Turkey. *Contributions to Mineralogy and Petrology* **79**, 361–367.

Özgenç, İ. & İlbeyli, N. 2008. Petrogenesis of the Late Cenozoic Eğrigöz pluton in western Anatolia (Turkey): implications for magma genesis and crustal processes. *International Geology Review* **50**, 375–391.

Ramsay, J. G. 1980. Shear zone geometry: a review. *Journal of Sructural Geology* **2**, 83–99.

Ring, U. & Collins, A.S. 2005. U-Pb SIMS dating of synkinematic granites: timing of core-complex formation in the northern Anatolide belt of western Turkey. *Journal of the Geological Society, London* **162**, 289–298.

Rudnick, R.L. & Goldstein, S.L. 1990. The Pb isotopic compositions of lower crustal xenoliths and the evolution of lower crustal Pb. *Earth and Planetary Science Letters* **98**, 192–207.

Schmidt, M.W. 1992. Amphibole composition in tonalite as a function of pressure: an experimental calibration of the Al-in-hornblende barometer. *Contributions to Mineralogy and Petrology* **110**, 304–310.

Seyitoğlu, G., Işık, V. & Çemen, İ. 2004. Complete Tertiary exhumation history of the Menderes massif, western Turkey: an alternative working hypothesis. *Terra Nova* **16**, 358–364.

Sibson, R.H. 1977. Fault rocks and fault mechanisms. *Journal of the Geological Society, London* **133**, 191–213.

Stouraiti, C., Mitropoulos, P., Tarney, J., Barreiro, B., Mcgrath, A.M. & Baltatzis, E. 2010. Geochemistry and petrogenesis of late Miocene granitoids, Cyclades, southern Aegean: nature of source components. *Lithos* **114**, 337–352.

Taylor, S.R. & Mclennan, S.M. 1985. *The Continental Crust: Its Composition and Evolution*. Blackwell, Oxford.

Tirel, C., Gautier, P., Van Hinsbergen, D.J.J. & Wortel, M.J.R. 2009. Sequential development of interfering metamorphic core complexes: numerical experiments and comparison with the Cyclades, Greece. *In*: Van Hinsbergen, D.J.J., Edwards, M. A. & Govers, R. (eds), *Collision and Collapse at the Africa–Arabia–Eurasia Subduction Zone*. Geological Society, London, Special Publications **311**, 257–292.

Thomson, S.N. & Ring, U. 2006. Thermochronologic evaluation of postcollision extension in the Anatolide orogen, western Turkey. *Tectonics* **25**, 1–20.

Tulloch, A.J. & Challis, G.A. 2000. Emplacement depths of Paleozoic–Mesozoic plutons from western New Zealand estimated by hornblende-Al geobarometry. *New Zealand Journal of Geology and Geophysics* **43**, 555–567.

Wilson M. 1989. *Igneous Petrogenesis*. Unwin Hyman Ltd., London, UK.

Yilmaz, Y., Genç, S.C., Karacik, Z. & Altunkaynak, S. 2001. Two contrasting magmatic associations of NW Anatolia and their tectonic significance. *Journal of Geodynamics* **31**, 243–271.

Yilmaz, Y. 2008. Main geological problems of Western Anatolia and the significance of the Bodrum magmatic province. Earth and Environmental Science **2** 012007, doi:10.1088/1755-1307/2/1/012007.